Eur. Phys. J. E **18**, 287–293 (2005)
DOI: 10.1140/epje/e2005-00034-9

THE EUROPEAN PHYSICAL JOURNAL E

Experimental realization of a model glass former in 2D

H. König[1,2,a], R. Hund[1,3], K. Zahn[1,4], and G. Maret[1]

[1] University of Konstanz, Department of Physics, 78457 Konstanz, Germany
[2] Johannes Gutenberg University of Mainz, Institute of Physics, 55099 Mainz, Germany
[3] Scintilla AG, 4501 Solothurn, Switzerland
[4] Ascom Systec Ltd., 5504 Mägenwil, Switzerland

Received 14 June 2005 / Received in final form 25 August 2005
Published online: 18 October 2005 –

Abstract. We have studied binary two-dimensional (2D) mixtures of superparamagnetic colloidal particles interacting through magnetic dipole moments, which were induced by an external magnetic field B. By tuning B the effective system temperature could be widely adjusted. Time-dependent particle coordinates measured by video-microscopy provide radial pair-distribution functions, mean-square displacements as well as evidence for heterogeneous dynamics. Characteristic features of 3D glass formers are observed experimentally in 2D for the first time.

PACS. 64.70.Pf Glass transition – 82.70.Dd Colloids – 83.10.Pp Particle dynamics

1 Introduction

The physical properties of glass formers in the supercooled or glassy state have been studied for more than a century. A glass can be considered as a solid with liquid-like structure, *i.e.* with no long-range order but with particle dynamics frozen-in at least at time scales of typical experiments [1]. So far no theory is capable to describe consistently all typical physical properties of glass formers [2,3]. Nevertheless, both the glass transition and the glassy state show universal features in many different atomic, molecular or macromolecular systems characterized by rather different interactions [4]. This might suggest that essential properties of glass formers can be understood by studying simple model systems.

According to this idea, substantial efforts were made recently to study three-dimensional (3D) colloidal glasses where individual particles are observed by confocal microscopy [5,6] or numerical simulations of different glass formers in 3D [7,8] and 2D [9]. In both cases time-dependent particle coordinates within the amorphous structures became directly available for the first time. These investigations together with the mode coupling theory [10–13] provided new insights especially into the particle dynamics in supercooled liquids and at the glass transition [14]. Nevertheless many questions remain, *e.g.* the origin of heterogeneous dynamics is still poorly understood.

In this paper, we report on the first *experimental* model system which shows special features of glass formers also in 2D [15]. Mixtures of superparamagnetic colloidal particles of two different sizes were confined by gravity to a flat horizontal water-air interface in a hanging drop geometry. The interparticle magnetic dipole interaction was controlled by a vertical magnetic field which sets the effective system temperature, T_{sys}. The particle's magnetic susceptibilities were independently determined. Thereby, the interaction is precisely calibrated. From time-dependent particle positions measured by video-microscopy partial radial pair-distribution functions, mean-square displacements as well as self-intermediate scattering functions were calculated. The close similarity of these functions with those of 3D glass formers indicates that our 2D colloidal system can be considered as a typical glass former [16,17]. Additional investigations of the microscopic particle dynamics using time-dependent particle coordinates show that heterogeneous dynamics and hopping processes are more pronounced at lower T_{sys}, *e.g.* when the liquid is more strongly supercooled. Connections between local less densely packed particle configurations and structural relaxations are mentioned. The local and ensemble averaged dynamics closely resembles that of 3D glass formers despite the fact that topological constraints and structural relaxation processes substantially differ in 2D and in 3D.

2 Experiment

PMMA colloids [18] of a polydispersity of about 3% used are doped with magnetite nano-crystals giving them a superparamagnetic behavior. The big (b) colloids (Dynabeads M-450, uncoated) have 4.7 μm diameter, a

[a] e-mail: koenigh@uni-mainz.de

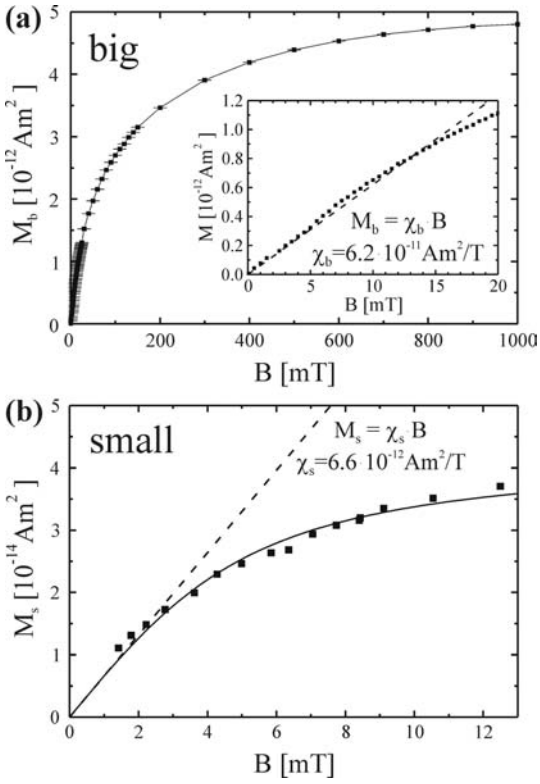

Fig. 1. Magnetic moment $M(B) = \chi(B) \cdot B$ of the big colloids (a) and small colloids (b) with a linear fit curve for low B-values (dashed lines) giving B-independent magnetic susceptibilities χ_s and χ_b used in the following. (a) From SQUID-measurement at room temperature. The line leads through the experimental points. (b) Comparison of data from the monodisperse small particles with Brownian-dynamics simulation [19]. The line represents a fit by a Langevin function, which is typical for (super-)paramagnetism [20].

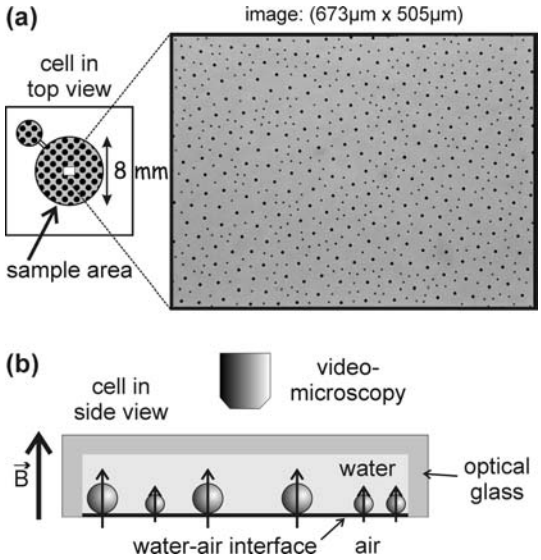

Fig. 2. Sketch of the experimental cell used to produce a flat water-air interface of hanging droplet geometry. (a) Top view, (b) side view. The liquid volume in the large cell was adjusted by adding/removing water in the small satellite cell connected to the main cell by a capillary. The binary colloidal monolayer was confined at the water-air interface by gravity. The induced magnetic moments are aligned by a vertical external magnetic field $\boldsymbol{B}$.

density $\rho_b \approx 1.5 \cdot 10^3\,\mathrm{kg/m^3}$ and a magnetic susceptibility $\chi_b = 6.2 \cdot 10^{-11}\,\mathrm{Am^2/T}$. The small (s) colloidal particles (dried Dynabeads M-280 uncoated) have a diameter of 2.8 μm, a density $\rho_s \approx 1.3 \cdot 10^3\,\mathrm{kg/m^3}$ and a magnetic susceptibility $\chi_s = 6.6 \cdot 10^{-12}\,\mathrm{Am^2/T}$. In Figure 1 the magnetic moments $M(B)$ of the big and small particles as a function of the applied magnetic field B are presented. In the range of B-values used (0 to $\approx$15 mT), χ_b remains constant, while χ_s decreases above 3 mT reaching about 84% of the low-B-value at 4 mT. In order to prevent aggregation, the big Dynabeads were stabilized by sodium dodecyl sulfonate (SDS) while the small Dynabeads were found to be stable in pure water [21]. Before mixing, the SDS rich suspension of the big colloids was removed by holding back the particles in the tube by a permanent magnet. Afterwards the big particles were also stable in pure water.

The colloidal suspension was filled into the flat cylindrical hole (height 1 mm) of a glass cell as sketched in Figure 2a. This cell was mounted upside down in a sample holder which consisted of a large copper block in order to reduce temperature gradients. The curvature of the drop suspended by interfacial tension, was reduced to unmeasurably small values by adjusting the water volume through a computer controlled nano-syringe. Thus the interface was tuned to a flatness of less than 1 μm at a cell diameter of 8 mm. Furthermore the horizontal orientation of the liquid-air interface itself was controlled through the adjustment of the optical table to $\pm 10^{-4}$ rad.

After sedimentation onto the free hanging water-air interface the colloids form a monolayer as sketched in Figure 2b. In fact, the system is almost ideally 2D: first, the gravitational length [22] of the big and small colloids is about 8 nm and 62 nm, respectively, much smaller than the particle diameters. Secondly, the gravitational force of the colloids is essentially unable to bulge the surface against the surface tension. Finally, vertical particle displacements due to capillary waves are less than $\sim$1 nm and thus negligible [23]. Collective particle drifts induced by flow of water, thermal gradients and disturbances of the water-air interface were minimized by surrounding the entire setup by a polystyrene box and laboratory air conditioning. A well equilibrated sample could be conserved for weeks and was stable enough to allow measurements over a period of about 24 hours.

An external homogeneous magnetic field, B, was applied perpendicular to the water-air interface by coils inducing vertical magnetic moments $\boldsymbol{M} = \chi \cdot \boldsymbol{B}$ in the particles. For such a geometry, induced magnetic moments interact pair-wise by a repulsive dipole-dipole potential proportional to B^2/r^3, r being the distance between the centers of two colloids. Because neighboring particles are typically separated by more than four times of their own diameter, deviations of the magnetic moments resulting

from the finite sizes of the particles can be neglected. We can also neglect the magnetic field generated by the induced magnetic moments of all other particles at the position of a given colloid. Contributions other than magnetic to the interaction potential between colloids, *e.g.* from electrostatics, are not significant as shown in [19].

The colloids in the monolayer undergo Brownian motion. Thus the system can be characterized by an interaction parameter, Γ, proportional to the ratio of the magnetic interaction potential $E_{\mathrm{m}}(B)$ to the thermal energy $k_{\mathrm{B}}T$. With the particle area density, ρ, related to the averaged particle distance by $\bar{r} = \rho^{-1/2}$, and with the number ratio ξ of the small to all particles, the Γ-value of the binary 2D colloidal mixture is given by:

$$\Gamma \;=\; \pi^{3/2}\frac{E_{\mathrm{m}}}{k_{\mathrm{B}}T} \;=\; \frac{\mu_0}{4\pi}\frac{B^2(\rho\pi)^{3/2}}{k_{\mathrm{B}}T}\left(\xi\cdot\chi_{\mathrm{s}} + (1-\xi)\cdot\chi_{\mathrm{b}}\right)^2 . \tag{1}$$

Since ρ and the temperature T remain constant during the experiment, Γ corresponds to an inverse system temperature, T_{sys}, which is tunable by B.

Typically 1000 particles out of approximately 100 000 in the cell were observed by video-microscopy, in a region far away from the cell edge (Fig. 2a) to avoid border effects. Time-dependent positions of all particles were determined in real-time by digitization on a frame grabber card and image processing on a PC. Every 0.25 s a complete set of uniquely labelled particle coordinates was determined and saved for evaluation later on: therefore, each video frame was converted into a binary image using a brightness cut-off value with the colloids represented as black discs on white background. The center of mass of a disc's area determined the corresponding particle position, which could be calculated with an accuracy of less than 0.2 μm. The disc's area indicated whether the particle is small or big. For the storage of a data set we used a multiple-τ-algorithm. In this algorithm, for the first multiple-τ-step, each analyzed data file is stored up to a fixed number max. In the second multiple-τ-step, only every other data file is stored, until max data files are available. For each following multiple-τ-step, the time-step between stored data files is again doubled. The multiple-τ-algorithm reduces the number of stored data files stepwise for increasing measuring time. This is appropriate for data plotting on a logarithmic time-scale.

Some uncertainties in the trajectories originate from slight drift effects caused by convective flow of water and from aggregates (normally ∼1%) having different magnetic susceptibilities and different diffusion coefficients. Although the drift was typically smaller than 1 μm/h, we minimized this effect by subtracting the average displacement of all particles from the displacement of each particle. The overall stability of the system itself was sufficiently good to obtain reliable data up to 10^5 s.

Summarizing this part, we would like to highlight several points showing why the experiment is an almost ideal 2D system for microscopic structural and dynamical investigations. The interaction of the magnetic moments of both monodisperse particle species, and hence T_{sys}, is calibrated. The repulsion is adjustable during the experiment from outside, which is not possible for hard-sphere or electrostatically interacting colloidal suspensions. The system is quite huge as compared to systems used in simulations allowing for measurements deep inside the bulk of the 2D system, where boundary effects are very small. Single particle tracking of the labelled colloids yields time-dependent particle coordinates, which allow to calculate averaged structural and dynamical functions as well as particle trajectories directly in the monolayer.

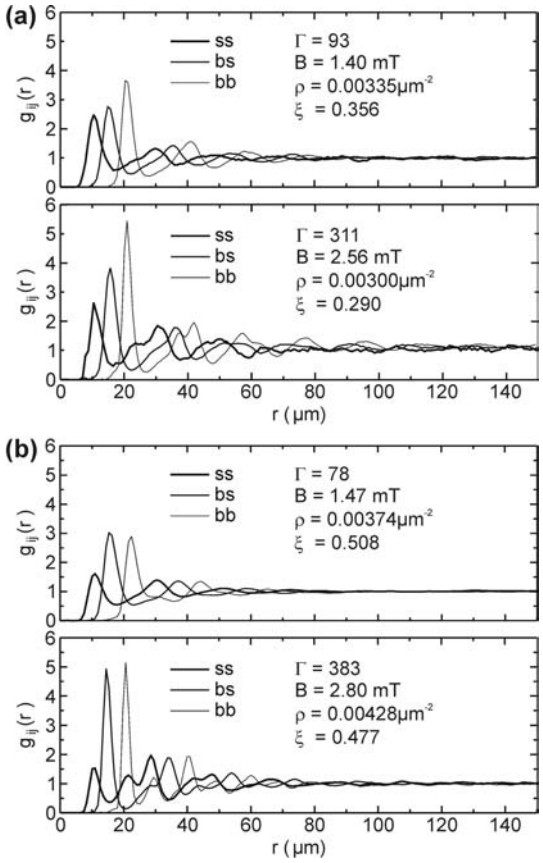

Fig. 3. Partial radial pair-distribution functions for $\xi \approx 0.3$ (a) and for $\xi \approx 0.5$ (b), both for a low and a high Γ-value.

3 Partial radial pair-distribution functions

The partial radial pair-distribution functions $g_{ij}(r)$ were calculated for the different pairs (ij) of big and small colloids by taking into account typically 100 independent particle configurations, in addition to the average over the approximately 1000 particles in the field of view presented in Figure 3.

Figure 3a shows measurements of $g_{ij}(r)$ for a binary 2D sample with relatively few small colloids ($\xi \approx 0.3$) at two different system temperatures Γ^{-1}. For increasing Γ, the first peaks of all partial $g_{ij}(r)$ become higher and narrower, the first minima decrease and a splitting of the second maxima becomes increasingly visible while no long-range order develops. Similar features are shown in

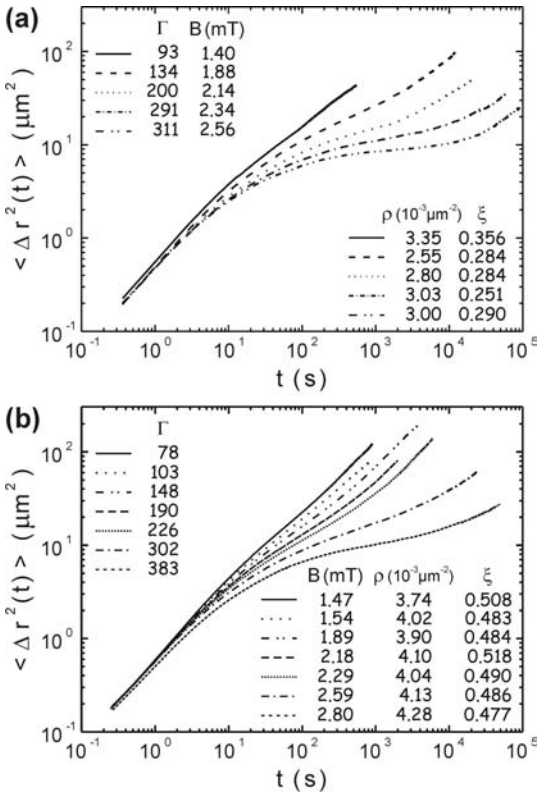

Fig. 4. Mean-square displacements averaged over big and small particles for samples with (a) $\xi \approx 0.3$ and (b) $\xi \approx 0.5$ for different $\Gamma = T_{\rm sys}^{-1}$ as indicated in the figure.

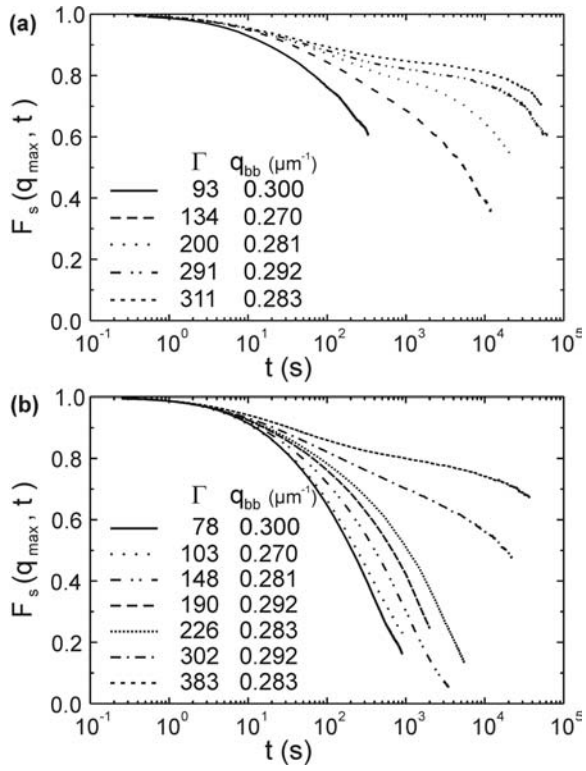

Fig. 5. Self-intermediate scattering functions averaged over big and small particles for samples with (a) $\xi \approx 0.3$ (see Fig. 4a) and (b) $\xi \approx 0.5$ (see Fig. 4b) for different $\Gamma = T_{\rm sys}^{-1}$.

Figure 3b for data at a higher fraction of small colloids ($\xi \approx 0.5$). These temperature-dependent changes of $g_{ij}(r)$ are typical "finger prints" of glass formers.

Several distinct local configurations of small and big particles can be observed in the binary 2D mixture [24]. The existence of four different local particle arrangements, one for each possible three particle combination of big and small colloids is shown in [24,25]. In [26] it is pointed out that the different peak positions of $g_{ij}(r)$ are related to these local packings and that their peak intensities strongly depend on composition of small and big particles.

Note that although monodisperse 2D systems form hexagonal crystals for $\Gamma > 60$ [27], the investigated binary systems (*i.e.* for ξ-values ranging between 0.3 and 0.7) remain entirely amorphous – at least over months – for considerably higher interaction parameters.

4 Dynamics of single particles

The 2D particle dynamics is directly quantified in real space by mean-square displacements, which are given by $\langle \Delta r^2(t) \rangle = \langle (\boldsymbol{r}_i(0) - \boldsymbol{r}_i(t))^2 \rangle$, considering the time-dependent position vectors $\boldsymbol{r}_i(t)$. In the analysis the average is performed over all particles i in the observed sample area for different multiple-τ-steps. The mean-square displacements of Figure 4 show a Γ-independent short-time behavior. For $t \leq 2\,\mathrm{s}$ the particles obey diffusive motion with a diffusion constant about 10% smaller than the free Stokes diffusion due to the hydrodynamic interaction near the liquid-air interface [19]. For longer time-scales, the slope of $\langle \Delta r^2(t) \rangle$ progressively diminishes for increasing Γ and a more pronounced plateau appears. As in atomic or molecular glasses this plateau is attributed to the so-called *cage effect*: the diffusive motion of the particles is hindered because of the surrounding particles. In the glassy state, the particles stay in their cages nearly for ever. In supercooled liquids, additional long-time α-relaxations lead to an increase of the mean-square displacements at long times since structural relaxations allow the particles to escape out of their cages.

Mean-square displacements of samples with a lot of aggregates [24] behave quite similar to those in Figure 4. This observation may suggest that relaxation processes in our system are not very sensitive to some polydispersity.

In Figure 5 we plot self-intermediate scattering functions $F_{\rm s}(q_{\rm max}, t) = \langle \exp(i q_{{\rm max},i} \cdot \Delta r_i(t)) \rangle$ for the data sets shown in Figure 4. $q_{{\rm max},i}$ denotes the scattering vector corresponding to the first maximum of $g_{ij}(r)$ of two big colloids. The $q_{{\rm max},i}$ values slightly change for the different curves because of density variations (see Fig. 4). The shape of $F_{\rm s}(q_{\rm max}, t)$ is rather similar to those measured in scattering experiments of 3D glass-formers [14]. Some disturbances of the long-time behavior of $\langle \Delta r^2(t) \rangle$ and $F_{\rm s}(q_{\rm max}, t)$ at high Γ can be attributed to heterogeneous dynamics or hopping processes, as we demonstrate later on.

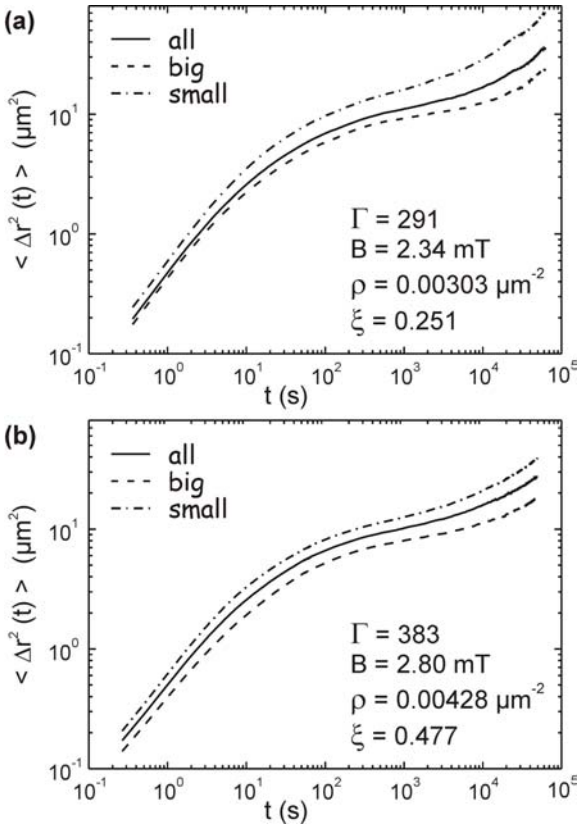

Fig. 6. Mean-square displacements of strongly supercooled liquids for big and small particles as well as averaged over all particles (compare with Fig. 4).

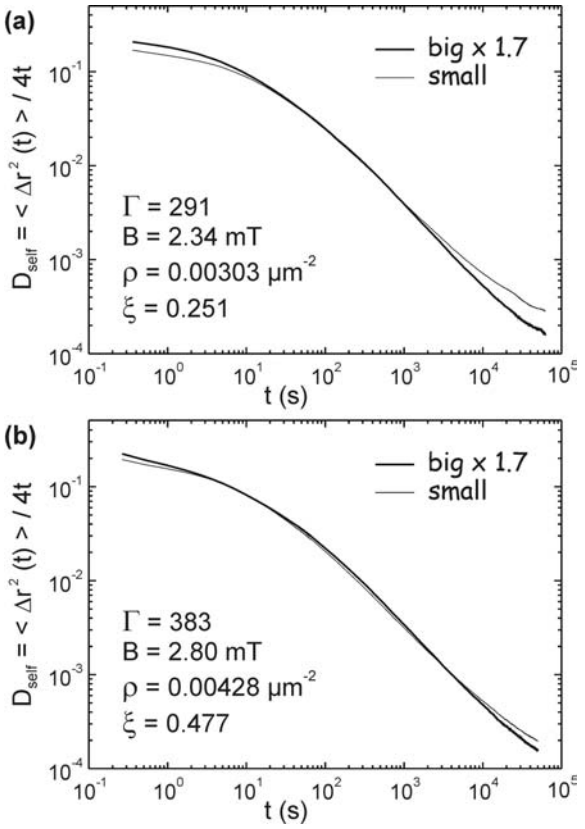

Fig. 7. Self diffusion coefficients D_{self} of strongly supercooled liquids. D_{self} of the big particles is additionally multiplied by 1.7 to get overlapping functions. Only for α-relaxation times, $D_{\mathrm{self,small}}$ becomes greater than $1.7 \cdot D_{\mathrm{self,big}}$, but the tendency of the dynamics is still the same, *i.e.* there is no dynamic phase separation for the different kinds of particles in strongly supercooled liquids.

In Figure 6 mean-square displacements are separately plotted for only big and only small colloids in contrast to all particles together. Qualitatively, big and small colloids move in the same way: the dynamical changes of both species happen in the same time-range, but the small particles are slightly faster than the big ones. In fact this difference seems to be accounted for by the difference in their self diffusion coefficients which amounts to about 1.7 (compare with Fig. 7). This, combined with visual inspection of particle trajectories in the next part, convincingly demonstrates that the system does not possibly separate into sub-phases containing, *e.g.* mainly solid big particles or liquid small particles, respectively. Furthermore, qualitatively identical behavior of $\langle \Delta r^2(t) \rangle$ was observed for all mixing ratios investigated ($0.3 < \xi < 0.7$). Different single particle friction coefficients also lead to the higher short-time diffusion of all particles the greater the number ratio ξ, as seen in Figure 4a for $\xi = 0.356$ compared to the other ones.

5 Microscopic relaxation dynamics of particle configurations

Particle trajectories of the binary colloidal 2D glass former are calculated from the time-dependent center-of-mass coordinates of the particles. Thus, structural dynamics in the monolayer can be studied at microscopic resolution. In Figure 8, 2-time particle trajectories are plotted connecting the initial and the final particle positions for the observation time ΔT by a straight line. The lengths and the directions of the neighboring 2-time trajectories reveal correlations of the particle movements in the monolayer.

Figure 8a shows 2-time particle trajectories of an isotropic liquid. For the chosen observation time ΔT the colloids were able to move on average over approximately a typical inter-particle distance. Slow particles are often found near by fast ones. Collective movements of several neighboring fast particles in one direction are rare.

In Figure 8b, 2-time particle trajectories of a mildly supercooled liquid are plotted. The observation time ΔT is chosen in the range of long-time α-relaxations, *e.g.* after the weakly pronounced plateau of the corresponding mean-square displacements (compare with Fig. 4a). The monolayer can be subdivided in regions of fast and directed collectively moving particles separated by areas of several particles with very little displacements, illustrating heterogeneous dynamics in the mildly supercooled state.

In Figure 9, time-resolved particle trajectories of a strongly supercooled liquid are plotted. The longest

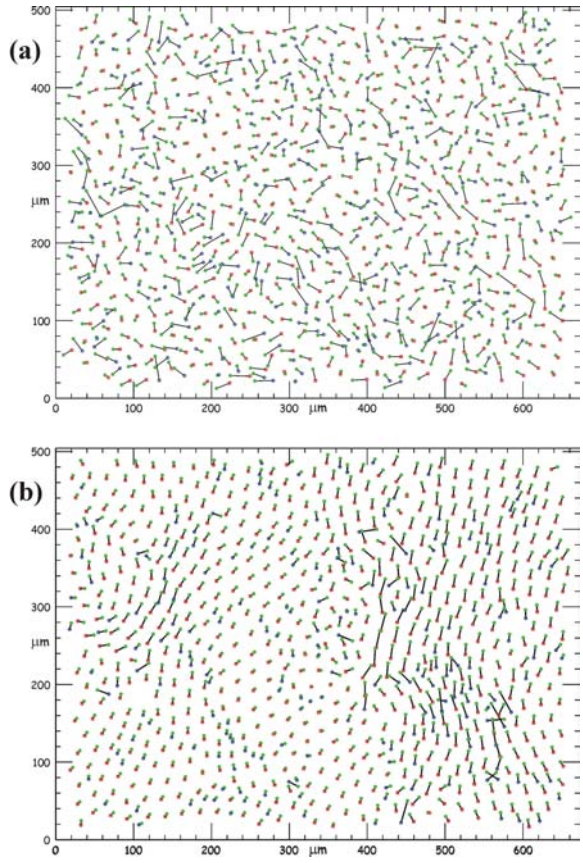

Fig. 8. 2-time particle trajectories. Red squares: initial positions of big colloids; blue circles: initial positions of small colloids; green discs: final particle positions. (a) Isotropic liquid: $\Gamma = 13.3$, $B = 0.685$ mT, $\rho = 2.73 \cdot 10^{-3} \mu\text{m}^{-2}$, $\xi = 0.43$, $\Delta T = 500$ s. (b) Supercooled liquid: $\Gamma = 134$, $B = 1.88$ mT, $\rho = 2.55 \cdot 10^{-3} \mu\text{m}^{-2}$, $\xi = 0.284$, $\Delta T = 3600$ s.

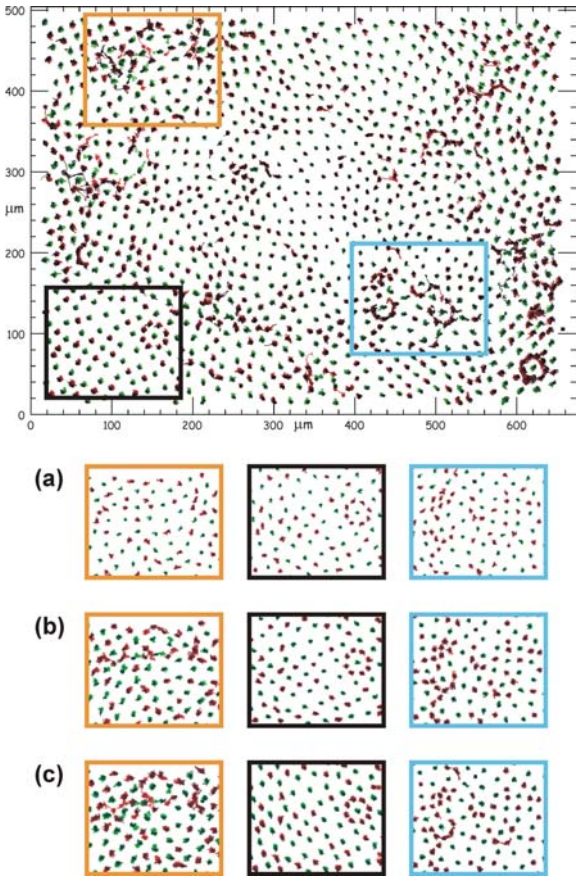

Fig. 9. Time-resolved particles trajectories of big (green) and small (red) colloids for a strongly supercooled liquid with $\Gamma = 383$, $B = 2.80$ mT, $\rho = 4.28 \cdot 10^{-3} \mu\text{m}^{-2}$, $\xi = 0.477$. The time development is additionally related to the brightness of the colors. Top: time step between two particle positions $\Delta t = 166$ s; time step for the whole observation: $\Delta T = 49\,761$ s. Bottom: time-resolved trajectories for three selected regions for smaller time steps. (a): $\Delta t = 1.3$ s, $\Delta T = 266$ s; (b): $\Delta t = 10.4$ s, $\Delta T = 3013$ s; (c): $\Delta t = 41.6$ s, $\Delta T = 12\,395$ s.

observation time ΔT lies in the range of α-relaxations after the clearly pronounced plateau of the corresponding mean-square displacements shown in Figure 4b. Strong heterogeneous dynamics is visible. Compared with Figure 8b, much more particle configurations remain locally stable. Only a low number of particles structurally relax mostly by string-like hopping processes where particles move in single file. Around those small areas where structural relaxations happen huge regions of local stable particle configurations exist. These time-dependent relaxation processes are typical for a strongly supercooled liquid. However, for such low system temperatures the observed area becomes too small to get useful statistics about the large-scaled heterogeneous dynamics. Thus, in the mean-square displacements of strongly supercooled liquids, shown in Figures 4 and 6, α-relaxations are typically disturbed.

In Figure 9, an interesting relation between heterogeneous dynamics and the local packing of colloidal particles can be qualitatively observed. A qualitative analysis of the connection between local structures and local dynamics will be subject of a forthcoming paper [28].

6 Conclusions

In comparison to other 2D and 3D glass formers studied so far, the uniqueness of our 2D colloidal binary system is that, exploiting time-dependent particle coordinates, local particle configurations can be investigated from the isotropic to strongly supercooled liquid state from short-time to long-time relaxations. Thus, the 2D binary colloidal suspensions with knob-tunable magnetic interparticle interactions are ideally suited to study structural and dynamic processes near the glass transition. For increasing $\Gamma = 1/T_{\text{sys}}$, the particle dynamics displays glassy slowing down as seen by an increased cage effect in the mean-square displacements and by heterogeneous dynamics. At the same time the local structure described by partial radial pair-distribution functions remains liquid-like with more pronounced short-range order. These properties give strong evidence that our system is the first experimental 2D glass former.

Summarizing the local relaxation processes, for decreasing system temperature the microscopic relaxation dynamics in supercooled liquids becomes more heterogeneous. For mildly supercooled systems, regions of fast particles move clearly cooperatively. For stronger supercooled liquids, the number of commonly moving particles decreases and finally there are separated regions of structural relaxations dominated by string-like hopping processes. The local particle dynamics in the 2D colloidal glass former resembles the heterogeneous dynamics found in 3D colloidal glass formers [5].

7 Outlook

Our results complement simulations [9] investigating 2D binary mixtures of soft discs [26]. However, our system allows to investigate local static and dynamic features of particle arrangements in great detail over time scales not accessible in numerical simulations. Corresponding work which highlights higher order correlations and the interplay of dynamic and structural heterogeneities will be published elsewhere [28]. The fact that regular elementary structures in 2D (such as triangular, square or rhombic particle arrangements) are much easier to detect than equivalent clusters in 3D allows to introduce a new concept which qualitatively describes the structural and dynamic properties of glass formers by conglomerations of local density-optimized formations [28].

It is still an open question whether one-component 2D systems can be quenched into a glassy state such as 3D ones. Marcus *et al.* investigated time-dependent particle coordinates of monodisperse uncharged spheres with nearly hard core interaction confining the colloidal particles between two glass plates while establishing equilibrium states of fixed volume fractions [29]. They found heterogeneous relaxations and string-like hopping for small volume fractions. Unfortunately, their set-up is not able to quench the system. In contrast, very high quench rates can be produced by the set-up presented here by increasing rapidly the external magnetic field.

We thank M. Lämmlin and Ch. Niedermaier for the Squid measurements shown in Figure 1. This work was supported by the Deutsche Forschungsgemeinschaft in the frame of SFB 513, project B6. We also acknowledge the Marie Curie Network RTN on Arrested Matter No. MRTN-CT-2003-504712.

References

1. M.D. Ediger, C.A. Angell, S.R. Nagel, J. Chem. Phys. **100**, 13200 (1996)
2. M. Mézard, Physica A **306**, 25 (2002)
3. R. Schilling, *Collective dynamics of nonlinear and disordered systems*, edited by G. Radons, W. Just, P. Häussler (Springer-Verlag, Berlin 2003), p. 153
4. T.A. Vilgis, *Disordered effects on relaxational processes*, edited by R. Richert, A. Blumen (Springer-Verlag, Berlin 1994), p. 153
5. E.W. Weeks, J.C. Crocker, A.C. Levitt, A. Schofield, D.A. Weitz, Science **287**, 627 (2000)
6. U. Gasser, A. Schofield, D.A. Weitz, J. Phys.: Condens. Matt. **15**, 375 (2003)
7. K. Binder, J. Baschnagel, W. Kob, W. Paul, *Bridging the time scales: molecular simulations for the next decade*, edited by P. Nielaba, M. Mareschal, G. Ciccotti (Springer-Verlag, Berlin 2002), p. 199
8. C. Donati, S.C. Glotzer, P.H. Poole, W. Kob, S.J. Plimpton, Phys. Rev. E **60**, 3107 (1999)
9. D.N. Perera, P. Harrowell, Phys. Rev. E **59**, 5721 (1999)
10. U. Bengtzelius, W. Götze, L. Sjögren, J. Phys. C **17**, 5915 (1984)
11. E. Leutheusser, Phys. Rev. A **29**, 2765 (1984)
12. W. Götze, L. Sjögren, in *Transport theory and statistical physics*, edited by S. Yip, P. Nelson (Dekker, 1995), p. 801
13. R. Schilling, J. Phys.: Condens. Matt. **12**, 6322 (2000)
14. W. van Megen, S.M. Underwood, Phys. Rev. E **49**, 4206 (1994)
15. M. Kollmann, R. Hund, B. Rinn, G. Nägele, K. Zahn, H. König, G. Maret, R. Klein J.K.G. Dhont, Europhys. Lett. **58**, 919 (2002)
16. T. Kondo, K. Tsumuraya, M.S. Watanabe, J. Chem. Phys. **93**, 5182 (1990)
17. H. Miyagawa, Y. Hiwatari, B. Bernu, J.P. Hansen, J. Chem. Phys. **88**, 3879 (1988)
18. DYNAL PARTICLES AS, `http://www.dynalbiotech.com`
19. K. Zahn, J.M. Mèndez-Alcaraz, G. Maret, Phys. Rev. Lett. **79**, 175 (1997)
20. A. Aharoni, *Introduction to the theory of ferromagnetism* (Clarendon Press, Oxford, 1996)
21. H. König, Ph.D. Thesis, University of Konstanz (2002)
22. The gravitational length is defined as $(1/2) \cdot k_{\mathrm{B}}T$ divided by the amount of the gravitational force of the particle
23. A. Wille, K. Zahn, F. Valmont, G. Maret, Europhys. Lett. **57**, 219 (2000)
24. H. König, K. Zahn, G. Maret, in *Proceeding of Slow Dynamics in Complex Systems, Sendai, 2003*, edited by M. Tokuyama, I. Oppenheim (AIP **708**, New York, 2004), p. 40
25. H. König, in *Proceeding of Slow Dynamics in Complex Systems, Sendai, 2003*, edited by M. Tokuyama, I. Oppenheim (AIP **708**, New York, 2004), p. 76
26. H. König, Europhys. Lett. **71**, 838 (2005)
27. K. Zahn, G. Maret, Phys. Rev. Lett. **85**, 3656 (2000)
28. H. König (to be published)
29. A.H. Marcus, J. Schofield, S.A. Rice, Phys. Rev. E **60**, 5725 (1999)